



HAL
open science

High-order fluid-structure interaction in 2D and 3D. Application to blood flow in arteries

Vincent Chabannes, Gonçalo Pena, Christophe Prud'Homme

► **To cite this version:**

Vincent Chabannes, Gonçalo Pena, Christophe Prud'Homme. High-order fluid-structure interaction in 2D and 3D. Application to blood flow in arteries. *Journal of Computational and Applied Mathematics*, 2013, 246, pp.1-9. 10.1016/j.cam.2012.10.006 . hal-00657622v2

HAL Id: hal-00657622

<https://hal.science/hal-00657622v2>

Submitted on 2 Feb 2012

HAL is a multi-disciplinary open access archive for the deposit and dissemination of scientific research documents, whether they are published or not. The documents may come from teaching and research institutions in France or abroad, or from public or private research centers.

L'archive ouverte pluridisciplinaire **HAL**, est destinée au dépôt et à la diffusion de documents scientifiques de niveau recherche, publiés ou non, émanant des établissements d'enseignement et de recherche français ou étrangers, des laboratoires publics ou privés.

High order fluid structure interaction in 2D and 3D

Application to blood flow in arteries

Vincent Chabannes^a, Gonçalo Pena^{b,**}, Christophe Prud'homme^{a,c,*}

^aUniversité Grenoble 1 / CNRS, Laboratoire Jean Kuntzman / UMR 5224. Grenoble, F-38041, France

^bCMUC, University of Coimbra, Largo D. Dinis, Apartado 3008, 3001-454 Coimbra, Portugal

^cUniversité de Strasbourg / CNRS, IRMA / UMR 7501. Strasbourg, F-67000, France

Abstract

This paper addresses the numerical approximation of Fluid Structure Interaction (FSI) problems through the Arbitrary Lagrangian Eulerian (ALE) framework, high order methods and a Dirichlet-Newmann approach for the coupling. The paper is divided in two main parts. The first part concerns the discretization method for the FSI problem. We introduce an improved ALE map, capable of handling curved geometries in 2D and 3D in an unified manner, that is based on a local differential operator. We also propose a minimal CIP stabilization term for the fluid discretization that accounts for a smaller computational effort, while stabilizing the flow regime. The second part is dedicated to validate our numerical strategy through a benchmark and some applications to blood flow in arteries.

Keywords: High order methods, Arbitrary Lagrangian Eulerian transformation, Fluid-Structure Interaction

1. Introduction

Over the last few years, we have been working on building a mathematical and computational framework for arbitrary order fluid-structure interaction, see [1–6], in 2D and 3D including using simplicial meshes with a wide range of applications and in particular in bio-mechanics, e.g. blood flows in arteries. In this paper we present the progress made since our last publications [1, 2] as well as a brief overview of the framework we have built so far.

Our computational framework builds upon FEEL++ [6, 7] which allows for arbitrary order cG and dG Galerkin methods (finite element, spectral elements, ...) in 1D, 2D and 3D on simplices and hypercubes. The computational domain can also be high order, that is to say, the elements are curved and in our case described by a geometrical transformation — from a straight element — which is a polynomial of degree greater than one. These high order meshes can be generated by GMSH [8] — up to order five in 2D and order four in 3D. — High order approximations come at a cost both in terms of implementation and computational points of view. The former is addressed by a very generic framework based on modern C++ programming (meta-programming, expression templates, ...) and a language mimicing the mathematical language. The latter is addressed by a careful implementation and optimisation, see [6].

We propose to solve the Fluid-Structure Interaction (FSI) problem in the Arbitrary Lagrangian Eu-

*Corresponding author

**Principal corresponding author

Email addresses: `vincent.chabannes@imag.fr` (Vincent Chabannes), `gpena@mat.uc.pt` (Gonçalo Pena), `christophe.prudhomme@imag.fr` (Christophe Prud'homme)

lerian (ALE) framework, wchi reads as: find $(\mathcal{A}_t, \mathbf{u}_f, p_f, \boldsymbol{\eta}_s)$ such that

$$\rho_f \frac{\partial \mathbf{u}_f}{\partial t} \Big|_{\mathbf{x}^*} - \operatorname{div}_{\mathbf{x}}(2\mu_f \mathbf{D}_{\mathbf{x}}(\mathbf{u}_f)) + \rho_f((\mathbf{u}_f - \mathbf{w}_f) \cdot \nabla_{\mathbf{x}}) \mathbf{u}_f + \nabla_{\mathbf{x}} p_f = 0, \quad \text{in } \Omega_f^t \times I \quad (1)$$

$$\operatorname{div}_{\mathbf{x}}(\mathbf{u}_f) = 0, \quad \text{in } \Omega_f^t \times I \quad (2)$$

$$\rho_s \frac{\partial^2 \boldsymbol{\eta}_s}{\partial t^2} - \nabla \cdot (\mathbf{F}_s \boldsymbol{\Sigma}_s) = 0, \quad \text{in } \Omega_s \times I \quad (3)$$

$$\mathbf{u}_f - \frac{\partial \boldsymbol{\eta}_s}{\partial t} \circ \mathcal{A}_t^{-1} = 0, \quad \text{on } \Gamma_{fsi}^t \quad (4)$$

$$\mathbf{F}_s \boldsymbol{\Sigma}_s \hat{\mathbf{n}}_s + J_{\mathcal{A}_t} \mathbf{F}_{\mathcal{A}_t}^{-T} \hat{\boldsymbol{\sigma}}_f \hat{\mathbf{n}}_f = 0, \quad \text{on } \Gamma_{fsi}^0 \quad (5)$$

where $\Omega_f^t = \mathcal{A}_t(\Omega_f^*)$ and Ω_s are the domains occupied by the fluid and structure, respectively, Ω_f^* is the ALE reference domain for the fluid, \mathbf{x}^* and \mathbf{x} denote the coordinate systems in Ω_f^* and Ω_f^t respectively, \mathbf{u}_f and p_f the velocity and pressure of the fluid, $\frac{\partial \mathbf{u}_f}{\partial t} \Big|_{\mathbf{x}^*}$ is the ALE time derivative, $\mathbf{D}_{\mathbf{x}}(\mathbf{u}_f)$ the fluid deformation tensor, $\boldsymbol{\eta}_s$ the displacement of the structure, $\mathbf{F}_s = \mathbf{I} + \nabla \boldsymbol{\eta}_s$ is the structure deformation tensor, $\boldsymbol{\Sigma}_s = \lambda_s (\operatorname{tr} \mathbf{E}_s) \mathbf{I} + 2\mu_s \mathbf{E}_s$ represents the second Piola-Kirchhoff stress tensor, Γ_{fsi}^t the interface boundary between the fluid and structure and \mathcal{A}_t is the continuous ALE map. These notations allow to define the stress tensor $\hat{\boldsymbol{\sigma}}_f = \boldsymbol{\sigma}_f \circ \mathcal{A}_t$ and the normal vector $\hat{\mathbf{n}}_f = \mathbf{n}_f \circ \mathcal{A}_t$ in the reference domain. We define also $\mathbf{F}_{\mathcal{A}} = \nabla \mathcal{A}$ and $J_{\mathcal{A}} = \det(\mathbf{F}_{\mathcal{A}})$. The problem is complemented with boundary conditions at the inflow Γ_{in} and outflow Γ_{out} . Since our motivation is driven by blood flow in arteries, we present in Figures 1 and 2 two simplified geometries that exemplify the domains and boundaries for the problem described above.



Figure 1: Two dimensional geometry

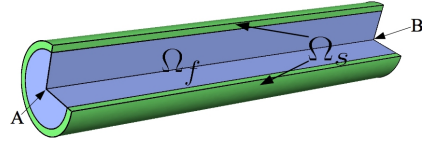


Figure 2: Three dimensional geometry

In [1] the authors have proposed a framework for high order (in space and time) fluid structure interaction in 2D using an efficient high order ALE map construction which is described in [2]. In this paper, we follow the same ALE framework. A fundamental ingredient in the ALE framework is the discrete ALE transformation that maps the reference configuration Ω_f^* onto the computational domain Ω_f^t at each timestep. The discrete ALE map proposed in [2] allows for an accurate description of the boundary of the computational domain, while inducing straight edges in the interior elements of the computational domain's mesh. However, this construction is based on the harmonic extension operator and Gordon-Hall transformations, see Gordon-Hall [9, 10]. The use of the harmonic extension can, if the mesh deformation is large enough, introduce invalid meshes in the computations, see Figure 3. As to the Gordon-Hall transformations, they make the extension of this ALE map intricate to three dimensional domains. To overcome these difficulties, we propose in this paper to replace the stage based on Gordon-Hall transformations, by the solution of a local differential problem in each element in contact with the curved boundary and the harmonic extension by the Winslow smoother (only in 2D), see [11]. The construction of this map shall be addressed in detail in section 3.

In the framework also presented in [2], the fluid flow is stabilized with the interior penalty method in the case of dominant convection terms. In the 2D and 3D blood flow applications presented in the paper, see section 6, even though stabilization is not necessary due to dominant convective terms, it is required to control the velocity at the inlet of the domain where Neumann conditions are imposed. In fact we propose to add minimal stabilization contributions, see section 4.

The paper is organized in the following way: first, in section 2, we introduce some definitions and notations needed to present the construction of the ALE map and the FSI framework addressed later in sections 3 and 4 respectively. Section 5 is devoted to validating the numerical method presented with

the benchmark [12]. Finally, we apply the methodology developed to two blood flow problems under realistic parameters, both in 2D and 3D, and using high order approximations.

2. Definitions and Notations

Let $\Omega \subset \mathbb{R}^d$, $d \geq 1$, denote a bounded connected domain and δ a discretisation parameter. We first need to introduce a suitable discretization of Ω , in general $\Omega_\delta \neq \Omega$. Note that if Ω is a polyhedral domain then $\Omega_\delta = \Omega$. We define $\hat{K} \subset \mathbb{R}^d$ $d = 1, 2, 3$ a reference elementary convex, e.g. a simplex or a hypercube. We denote by \mathcal{T}_δ a finite collection of nonempty, disjoint open simplices or hypercubes $\mathcal{T}_\delta \equiv \mathcal{T}_{(h,k)} = \{K = \varphi_{K,k}^{\text{geo}}(\hat{K})\}$ forming a partition of Ω_δ such that $h = \max_{K \in \mathcal{T}_\delta} h_K$, with h_K denoting the diameter of the element $K \in \mathcal{T}_\delta$ and $\varphi_{K,k}^{\text{geo}}$ is the polynomial of degree k that maps \hat{K} to K which also called the geometric transformation. We say that a hyperplanar closed subset F of $\overline{\Omega_\delta}$ is a mesh face if it has positive $(d-1)$ -dimensional measure and if either there exist $K_1, K_2 \in \mathcal{T}_\delta$ such that $F = \partial K_1 \cap \partial K_2$ (and F is called an *internal face*) or there exists $K \in \mathcal{T}_\delta$ such that $F = \partial K \cap \partial \Omega_\delta$ (and F is called a *boundary face*). Internal faces are collected in the set \mathcal{F}_δ^i , boundary faces in \mathcal{F}_δ^b and we let $\mathcal{F}_\delta := \mathcal{F}_\delta^i \cup \mathcal{F}_\delta^b$. For all $F \in \mathcal{F}_\delta$, we define $\mathcal{T}_F := \{K \in \mathcal{T}_\delta \mid F \subset \partial K\}$. For every interface $F \in \mathcal{F}_\delta^i$ we introduce two associated normals to the elements in \mathcal{T}_F and we have $\mathbf{n}_{K_1,F} = -\mathbf{n}_{K_2,F}$, where $\mathbf{n}_{K_i,F}$, $i \in \{1, 2\}$, denotes the unit normal to F pointing out of $K_i \in \mathcal{T}_F$. On a boundary face $F \in \mathcal{F}_\delta^b$, $\mathbf{n}_F = \mathbf{n}_{K,F}$ denotes the unit normal pointing out of Ω_δ .

Without loss of generality we suppose from now on that we work with simplicial elements. Given a positive integer N , we denote by $\mathbb{P}^N(\hat{K})$ and $\mathbb{P}^N(K)$ the spaces of polynomials of total degree less or equal than N defined in \hat{K} and K respectively. From now on Ω_δ is called the *computational* domain and we introduce Ω_δ^* which will be referred as the *reference* domain. We assume that the reference domain has a straight edge/face mesh associated i.e. $\mathcal{T}_\delta^* \equiv \mathcal{T}_{(h,1)}$. Furthermore we admit that the mesh \mathcal{T}_δ^* covers exactly the domain Ω_δ^* , i.e., $\Omega_\delta^* = \bigcup_{K^* \in \mathcal{T}_\delta^*} \overline{K^*}$. We denote $\mathcal{A}_\delta \equiv \mathcal{A}_{(h,k)}$ a transformation that maps Ω_δ^* to Ω_δ which we later call the ALE discrete map.

We define $P_c^N(\Omega_\delta^* \equiv \Omega_{(h,1)}^*)$ and $[P_c^N(\Omega_\delta^* \equiv \Omega_{(h,1)}^*)]^d$ the spaces of continuous scalar and vectorial functions respectively on Ω_δ^* as follows:

$$P_c^N(\Omega_\delta^*) = \{v \in C^0(\Omega_\delta^*) \mid v \circ \varphi_{K,1}^{\text{geo}} \in \mathbb{P}^N(\hat{K}) \forall K \in \mathcal{T}_\delta^*\}, \quad [P_c^N(\Omega_\delta^*)]^d = \prod_1^d P_c^N(\Omega_\delta^*). \quad (6)$$

We define similarly $P_c^N(\Omega_\delta \equiv \Omega_{(h,k)})$ and $[P_c^N(\Omega_\delta \equiv \Omega_{(h,k)})]^d$ with $k \geq 1$ similarly:

$$P_c^N(\Omega_\delta) = \{v \in C^0(\Omega_\delta) \mid v \circ \varphi_{K,k}^{\text{geo}} \in \mathbb{P}^N(\hat{K}) \forall K \in \mathcal{T}_\delta\}, \quad [P_c^N(\Omega_\delta)]^d = \prod_1^d P_c^N(\Omega_\delta). \quad (7)$$

Finally let us denote by $\boldsymbol{\eta} : \partial \Omega_\delta^* \rightarrow \partial \Omega_\delta$ a displacement function. Through $\boldsymbol{\eta}$, we classify three subsets of the boundary: (i) Γ_M^* , the portion of the boundary that moves according to the displacement $\boldsymbol{\eta}$, (ii) Γ_F^* , the portion of the boundary that stays fixed (ie, $\boldsymbol{\eta}(\mathbf{s}) = \mathbf{s}, \forall \mathbf{s} \in \Gamma_F^*$) and (iii) Γ_N^* , the part of the boundary on which we do not prescribe a displacement. The image of each subset, Γ_M^* , Γ_F^* and Γ_N^* by $\boldsymbol{\eta}$ is denoted by Γ_M, Γ_F and Γ_N , respectively. These three sets do not overlap and they verify $\partial \Omega_\delta^* = \overline{\Gamma_M^*} \cup \overline{\Gamma_F^*} \cup \overline{\Gamma_N^*}$. Denote $\mathcal{T}_\delta^{*,b} = \{K^* \in \mathcal{T}_\delta^* : \partial K^* \cap \Gamma_M^* \neq \emptyset\}$ the set of elements K^* sharing a face with the boundary of Ω_δ^* .

3. High order ALE transformation

In both papers [1, 2], the piecewise linear map created is calculated by performing first a harmonic extension (or modified harmonic extension) of the boundary data. However, if the displacement is too large, these operators can induce meshes that are not valid due to, for instance, *mesh folding*. A way to circumvent this problem, that stems from the structure of the proposed ALE map construction, is to replace the harmonic extension by a more suitable and flexible operator that avoids these issues or

improves the mesh quality. An example of such an operator for two dimensional domains is the Winslow smoother [11]. From a continuous point of view, the Winslow smoother enforces that the inverse of the ALE map is harmonic, not the map itself. This accounts for solving a quasi-linear system of PDEs,

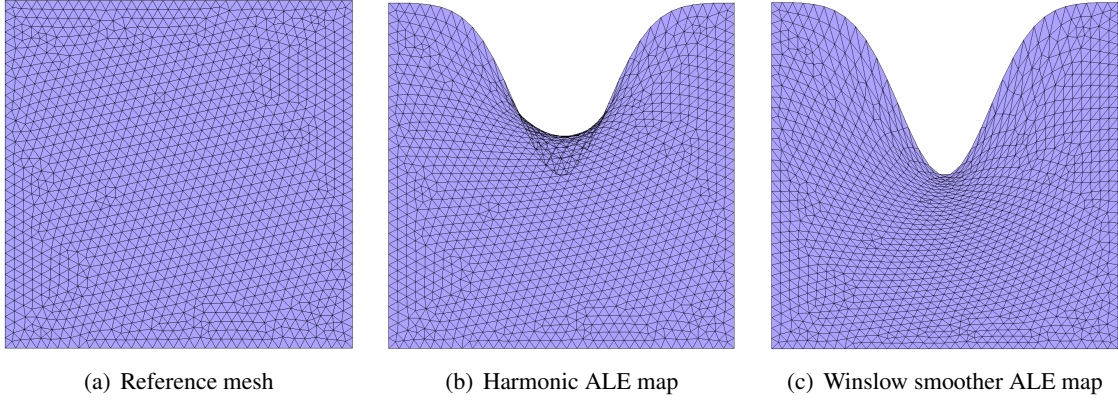


Figure 3: Comparison of first order meshes generated by the harmonic extension (invalid) and Winslow smoother (valid) operators respectively

which can be done using fixed point or Newton iterations. Figure 3 displays the effect of the harmonic extension and the Winslow smoother for the same imposed displacement at the top of the unit square, see [13]. In 3D, we maintain the harmonic extension operator.

We suppose from now on that only the elements touching the boundary are curved while the elements in the interior are straight — the geometric transformation associated is affine. — The construction of the ALE map is then done in two steps: the first step is to use the Winslow smoother to extend the displacement $\boldsymbol{\eta}$ to the interior of the reference domain using piecewise linear polynomial functions and obtain the corresponding ALE transformation, $\mathcal{A}_{(h,1)}$. The second step is a correction performed in each element that touches the curved boundary in order to build a high order approximation. In each element $K^* \in \mathcal{T}_{(h,1)}^{*,b}$ we look for $\mathcal{A}_{(h_{K^*},N)} \in [\mathbb{P}^N(K^*)]^d$ such that

$$\begin{cases} \int_{K^*} \nabla \mathcal{A}_{(h_{K^*},N)} : \nabla \mathbf{z} \, dx = 0, & \forall \mathbf{z} \in [\mathbb{P}^N(K^*)]^d \\ \mathcal{A}_{(h_{K^*},N)}(\mathbf{x}^*) = \boldsymbol{\eta}(\mathbf{x}^*) + \mathbf{x}^* - \mathcal{A}_{(h,1)}(\mathbf{x}^*), & \forall \mathbf{x}^* \in \partial K^* \cap \Gamma_M^* \\ \mathcal{A}_{(h_{K^*},N)} = \mathbf{0}, & \text{elsewhere on } \partial K^*. \end{cases}$$

where Γ_M^* is the portion of boundary in the reference domain that is curved in the computational domain. The final ALE map, $\mathcal{A}_\delta \equiv \mathcal{A}_{(h,N)}$ is obtained by adding to $\mathcal{A}_{(h,1)}$ the correction $\mathcal{A}_{(h_{K^*},N)}$ on each element of $\mathcal{T}_{(h,1)}^{*,b}$

$$\mathcal{A}_{(h,N)}(\mathbf{x}^*) = \mathcal{A}_{(h,1)}(\mathbf{x}^*) + \sum_{K^* \in \mathcal{T}_{(h,1)}^{*,b}} \mathcal{A}_{(h_{K^*},N)}(\mathbf{x}^*) + \mathbf{x}^*$$

Conjecture 1 (Properties of $\mathcal{A}_{(h,N)}$). *Under the previous assumptions and by construction, $\mathcal{A}_{(h,N)} \in [P_c^N(\mathcal{T}_{(h,1)}^{*,b})]^d$ — enjoys optimal approximation properties i.e. the boundary approximation is $\mathcal{O}(h^{N+1})$ in the L^2 -norm — and $\mathcal{A}_{(h,N)} \in [P_c^1(\mathcal{T}_{(h,1)}^* \setminus \mathcal{T}_{(h,1)}^{*,b})]^d$.*

We present now some numerical experiments to verify Conjecture 1. We consider the reference domain depicted in Figure 4(a) defined by

$$\Omega^{*,cy} = \left\{ (x^*, y^*, z^*) \in \mathbb{R}^3 : x^* \in [0, 5], y^{*2} + z^{*2} \leq 0.5^2 \right\}$$

and the associated displacement of its boundary $\boldsymbol{\eta}^{cy}(\mathbf{x}^*) = 0.2 \exp\left(\frac{x^*}{5}\right) \sin\left(\frac{\pi x^*}{2.5}\right) \mathbf{n}^*$. Figure 4(b) displays the computational domains colored by the corresponding ALE map.

Finally, Figure 4(c) displays the convergence rate of the quantity $\|\mathcal{A}_{(h,N)}(\mathbf{x}^*) - (\mathbf{x}^* + \boldsymbol{\eta}(\mathbf{x}^*))\|_{[L^2(\Gamma_M^*)]^d}$ which confirms the result of Conjecture 1 with respect to geometric order N .

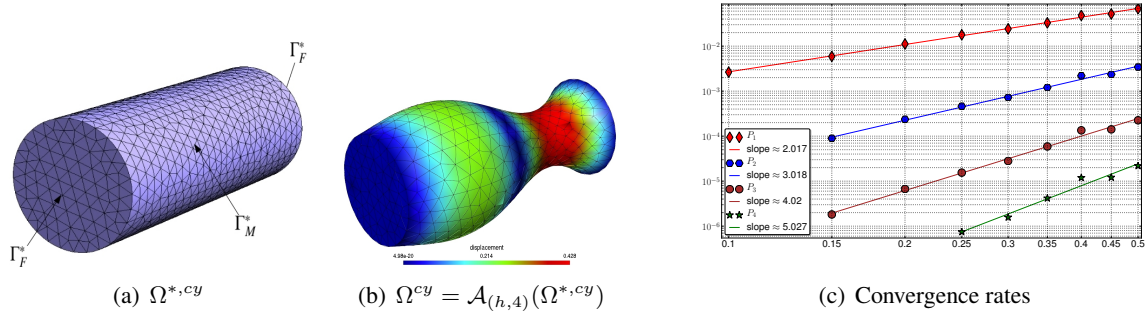


Figure 4: Reference (left) and computational (center) meshes of order 4 displayed using GMSH colored by the displacement's magnitude. Convergence rate plots of $\mathcal{A}_{(h,N)}$, $N = 1, 2, 3, 4$ with respect to h (right).

4. Discretization method

We introduce now the numerical method used to solve the FSI problem. We use a Dirichlet-Neumann approach for the coupled FSI problem. This accounts for using a fixed point method, iterating between solves of the fluid equations and solves of the structure equations with appropriate Dirichlet and Neumann boundary conditions respectively. For the fluid solver, we use the same numerical methods as in [2] which we review very briefly in the next section as well as the structure solver afterwards.

4.1. Fluid discretization

We start by introducing some notations. Let $\Omega_{f,(h,1)}^*$ denote the reference domain, constructed from the high order mesh (with geometrical transformations of degree k) of the domain occupied by the fluid at time t_0 by straightening all interior edges and faces (note that as a consequence, this domain is a polyhedron). We define $\Omega_{f,\delta}^t := \mathcal{A}_{\delta}^t(\Omega_{f,(h,1)}^*)$ which is partitioned by a high order mesh. With these notations, the fluid problem reads as: for each $n \geq 1$, we look for the solution $(\mathbf{u}_{\delta}^{n+1}, p_{\delta}^{n+1}) \in [P_c^N(\Omega_{f,\delta}^t)]^d \times P_c^{N-1}(\Omega_{f,\delta}^t)$, with $\mathbf{u}_{\delta}^0 = \mathbf{u}_{0,\delta}$ in $\Omega_{f,\delta}^{t_0}$, such that

$$\begin{aligned} \rho_f \frac{\beta_{-1}}{\Delta t} (\mathbf{u}_{\delta}^{n+1}, \mathbf{v}) + a(\mathbf{u}_{\delta}^{n+1}, \mathbf{v}) + s(\mathbf{u}_{\delta}^{n+1}, \mathbf{v}; \mathbf{u}_{\delta}^*) \\ - b(\mathbf{v}, p_{\delta}^{n+1}) + c(\mathbf{u}_{\delta}^{n+1}, \mathbf{v}; \mathbf{u}_{\delta}^* - \mathbf{w}_{\delta}^{n+1}) = (\tilde{\mathbf{f}}_{\delta}^{n+1}, \mathbf{v}), \quad \forall \mathbf{v} \in [P_c^N(\Omega_{f,\delta}^{t_{n+1}})]^d \\ b(\mathbf{u}_{\delta}^{n+1}, q) = 0, \quad \forall q \in P_c^{N-1}(\Omega_{f,\delta}^{t_{n+1}}) \end{aligned} \quad (8)$$

where

$$\begin{aligned} a(\mathbf{u}_{\delta}^n, \mathbf{v}) &= \int_{\Omega_{f,\delta}^{t_n}} \mathbf{D}_x(\mathbf{u}_{\delta}^n) : \nabla \mathbf{v} dx, \quad b(\mathbf{v}, p_{\delta}^n) = \int_{\Omega_{f,\delta}^{t_n}} \text{div}_x(\mathbf{v}) p_{\delta}^n dx \\ (\mathbf{u}_{\delta}^n, \mathbf{v}) &= \int_{\Omega_{f,\delta}^{t_n}} \mathbf{u}_{\delta}^n \cdot \mathbf{v} dx, \quad c(\mathbf{u}_{\delta}^n, \mathbf{v}; \boldsymbol{\beta}) = \rho_f \int_{\Omega_{f,\delta}^{t_n}} [\boldsymbol{\beta} \cdot \nabla_x] \mathbf{u}_{\delta}^n \cdot \mathbf{v} dx \\ s(\mathbf{u}_{\delta}^n, \mathbf{v}; \boldsymbol{\beta}) &= \gamma \sum_{F \in \mathcal{F}} \int_F |\boldsymbol{\beta} \cdot \mathbf{n}| \frac{h_F^2}{N^{3.5}} \llbracket \nabla \mathbf{u}_{\delta}^n \rrbracket_F \cdot \llbracket \nabla \mathbf{v} \rrbracket_F ds, \end{aligned}$$

β_{-1} and $\tilde{\mathbf{f}}_{\delta}^{n+1}$ are determined according to the corresponding BDF method, \mathcal{F} denotes a set of faces and $\llbracket \cdot \rrbracket_F$ denotes the jump across the face F , \mathbf{u}_{δ}^* is an extrapolated velocity and $\mathbf{w}_{\delta}^{n+1}$ is the mesh velocity. See [2] for a complete description of all variables. At each iteration of the fix point method, this problem is subject to Dirichlet boundary conditions in the moving interface of the domain and Neumann boundary conditions in the inlet and outlet (these are incorporated through the force term $\tilde{\mathbf{f}}_{\delta}^{n+1}$).

In [2] the authors proposed $\mathcal{F} = \mathcal{F}_h^i$, i.e., the use of all internal faces in the calculation of $s(\mathbf{u}_\delta^n, \mathbf{v}; \boldsymbol{\beta})$. We propose two alternatives which reduce considerably the computational effort, while still stabilizing the flow regime in blood flow simulations, see section 6. They are (i) $\mathcal{F} = \Gamma_{in} \cap \mathcal{F}_h^b$ for only the faces at the inlet and (ii) $\mathcal{F} = \mathcal{F}_h^i \cap \{\mathbf{x} \in \mathbb{R}^d : (\mathbf{x}_{in} - \mathbf{x}, \mathbf{n}_{in}) \leq 0\}$, for a set of faces close to the inlet, where \mathbf{x}_{in} is a suitable point inside the computational domain and \mathbf{n}_{in} is the outward normal to Γ_{in} .

4.2. Structure discretization

We start this section by introducing the notation for the reference domain for the structure, $\Omega_{s,\delta}$, as well as the discrete space

$$V_{s,\delta}^N \equiv V_{s,(h,k)}^N = \left\{ \boldsymbol{\eta}_s \in [P_c^N(\Omega_{s,\delta} \equiv \Omega_{s,(h,k)})]^d, \quad \boldsymbol{\eta}_s = \mathbf{0} \text{ on } \Gamma_{in} \text{ and } \Gamma_{out} \right\}. \quad (9)$$

where $N \geq 1$ and $k \geq 1$. Given a displacement function $\boldsymbol{\eta}_s \in V_{s,\delta}^N$, we introduce the structure configuration at time t as $\Omega_s^t = (\mathbf{I} + \boldsymbol{\eta}_s)(\Omega_{s,\delta})$.

Using a Newmark scheme for the time discretisation at each time step t_n , we define the displacement $\boldsymbol{\eta}_{s,\delta}^n$ and its time derivatives $\dot{\boldsymbol{\eta}}_{s,\delta}^n$ and $\ddot{\boldsymbol{\eta}}_{s,\delta}^n$, all belonging to space $V_{s,\delta}^N$. Moreover, we enforce that the velocity and acceleration discretisations are functions of the previous time steps

$$\ddot{\boldsymbol{\eta}}_{s,\delta}^{n+1} = \frac{1}{\beta \Delta t^2} (\boldsymbol{\eta}_{s,\delta}^{n+1} - \boldsymbol{\eta}_{s,\delta}^n) - \frac{1}{\beta \Delta t} \dot{\boldsymbol{\eta}}_{s,\delta}^n - \left(\frac{1}{2\beta} - 1 \right) \ddot{\boldsymbol{\eta}}_{s,\delta}^n \quad (10)$$

$$\dot{\boldsymbol{\eta}}_{s,\delta}^{n+1} = \frac{\gamma}{\beta \Delta t} (\boldsymbol{\eta}_{s,\delta}^{n+1} - \boldsymbol{\eta}_{s,\delta}^n) - \left(\frac{\gamma}{\beta} - 1 \right) \dot{\boldsymbol{\eta}}_{s,\delta}^n - \Delta t \left(\frac{\gamma}{2\beta} - 1 \right) \ddot{\boldsymbol{\eta}}_{s,\delta}^n \quad (11)$$

The two parameters γ and β are taken to be $\gamma = 0.5$ and $\beta = 0.25$ to ensure unconditional stability of the Newmark scheme. The discrete variational formulation leads to finding $\boldsymbol{\eta}_{s,\delta}^{n+1} \in V_{s,\delta}^N$ for all time step t_{n+1} such as:

$$\int_{\Omega_{s,\delta}} \rho_s \ddot{\boldsymbol{\eta}}_{s,\delta}^{n+1} \cdot \boldsymbol{\xi}_s dx + \int_{\Omega_{s,\delta}} \left(\mathbf{F}_{s,\delta}^{n+1} \boldsymbol{\Sigma}_{s,\delta}^{n+1} \right) : \nabla \boldsymbol{\xi}_s dx = \int_{\Gamma_{fsi}^0} \mathbf{g}_s \cdot \boldsymbol{\xi}_s ds, \quad \forall \boldsymbol{\xi}_s \in V_{s,\delta}^N \quad (12)$$

where $\mathbf{g}_s = J_{A,\delta} \mathbf{F}_{A,\delta}^{-T} \hat{\boldsymbol{\sigma}}_{f,\delta} \hat{\mathbf{n}}_f$ is the stress induced by the fluid.

4.3. Solution strategy

The algebraic systems arising from the discretization proposed in the previous section are solved using a Newton or quasi-Newton algorithm with a cubic line search method. At each step, the linear solver applies the GMRES method with a LU preconditioner. The preconditioner is typically built only once throughout the nonlinear iterations unless the nonlinearity is too stiff and the preconditioner needs to be recalculated during the non-linear iterations. In the quasi-Newton instance, the Jacobian can be rebuilt once in a while during the nonlinear iterations or just once, which is often preferred when simulating time-dependent problems. The underlying framework for the linear and nonlinear solvers is PETSc [14].

5. Validation

We now present a FSI benchmark presented in [12] to validate our numerical strategy. This benchmark is a simulation of a flow in a rectangular domain with a rigid obstacle, a cylinder, and an elastic beam clamped to the cylinder. The benchmark configuration is taken from [12]. We monitor the lift and drag around the cylinder and the flag in Figures 5(c)-5(d) as well as the displacement of a point on the flag in Figures 5(a)-5(b). We compare our results with the ones provided in [12] which we denote **REF**.

The results are in accordance with reference values even though we used a really coarse mesh, thanks to the high order approximations, compared to the configuration in [12], see Table 5 and Figure 6. Only the lift is not in very good agreement: some little perturbations appear when we decrease the time step (cases **(1)** and **(2)**) and it seems to be caused by the time scheme (here a BDF of order 2).

	$x \times 10^{-3}$	$y \times 10^{-3}$	Drag	Lift
REF	-2.69 ± 2.53 [10.9]	1.48 ± 34.38 [5.3]	457.3 ± 22.66 [10.9]	2.22 ± 149.78 [5.3]
(1)	-2.90 ± 2.77 [11.0]	1.33 ± 34.90 [5.5]	457.9 ± 31.79 [11.0]	8.93 ± 216.21 [5.5]
(2)	-3.29 ± 3.12 [11.0]	1.0 ± 37.21 [5.5]	461.9 ± 33.44 [11.0]	-4.34 ± 188.00 [5.5]
(3)	-2.78 ± 2.69 [11.0]	1.55 ± 33.87 [5.5]	459.8 ± 31.06 [11.0]	-2.19 ± 174.45 [5.5]

Table 1: Results for **FSI3**

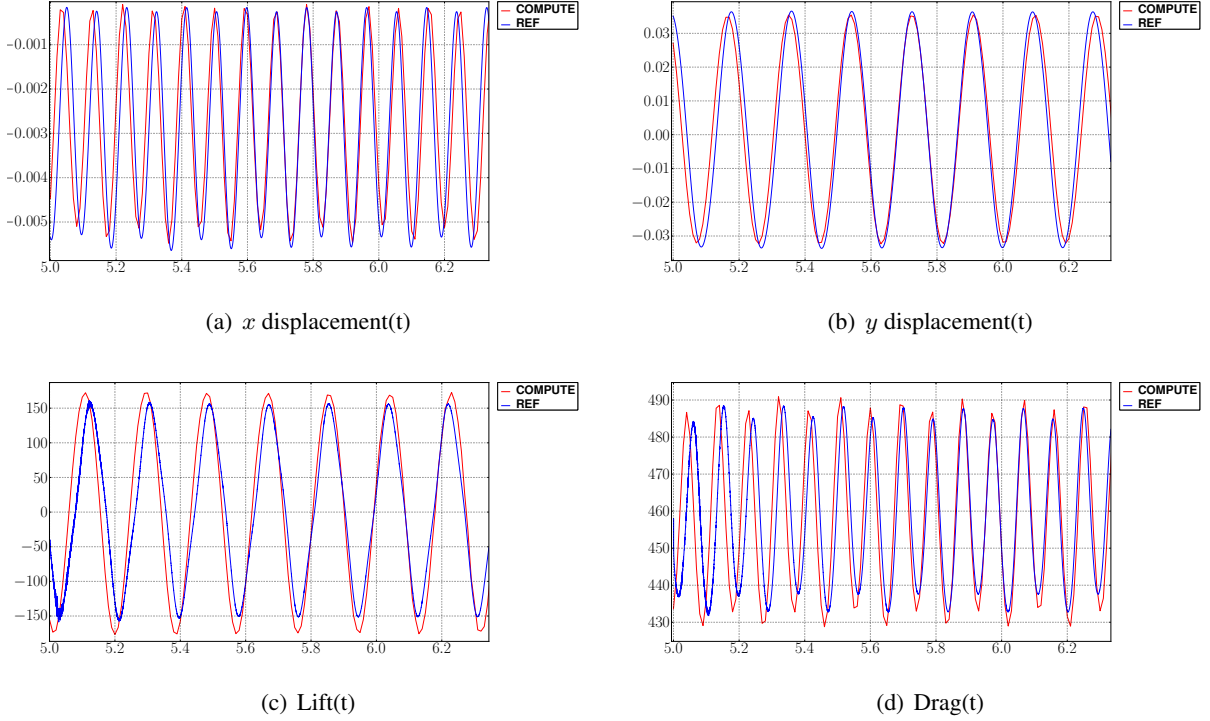


Figure 5: Results for **FSI3** with the configuration **(3)** in Table 5

	N_{elt}	N_{dof}	$[P_c^N(\Omega_{f,\delta})]^2 \times P_c^{N-1}(\Omega_{f,\delta}) \times V_{s,\delta}^N$	Δt
REF	15872	304128		0.0005
(1)	21930	86256	$[P_c^2(\Omega_{f,(h,1)})]^2 \times P_c^1(\Omega_{f,(h,1)}) \times V_{s,(h,1)}^1$	0.0005
(2)	1486	15492	$[P_c^3(\Omega_{f,(h,2)})]^2 \times P_c^2(\Omega_{f,(h,2)}) \times V_{s,(h,2)}^2$	0.001
(3)	1486	28823	$[P_c^4(\Omega_{f,(h,3)})]^2 \times P_c^3(\Omega_{f,(h,3)}) \times V_{s,(h,3)}^3$	0.01

Table 2: Benchmark configurations for **FSI3**

Finally, with the Figures 7(a) and 7(b), we show two screenshots of this benchmark.

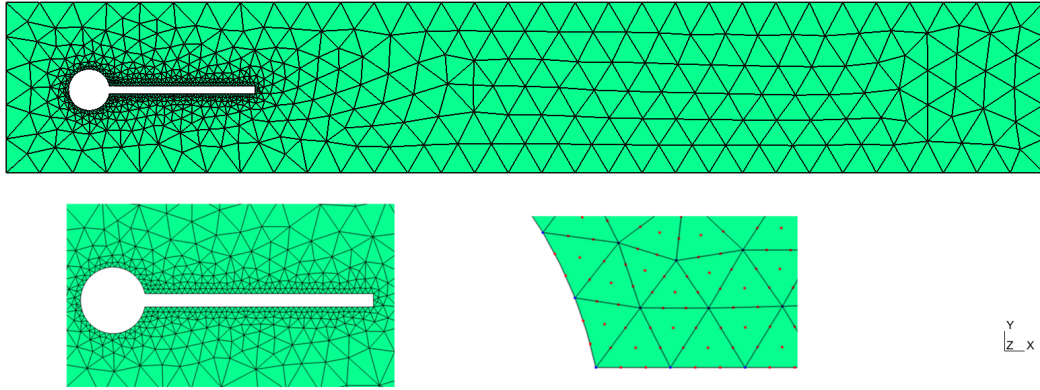


Figure 6: Reference mesh used for (3) in table 5

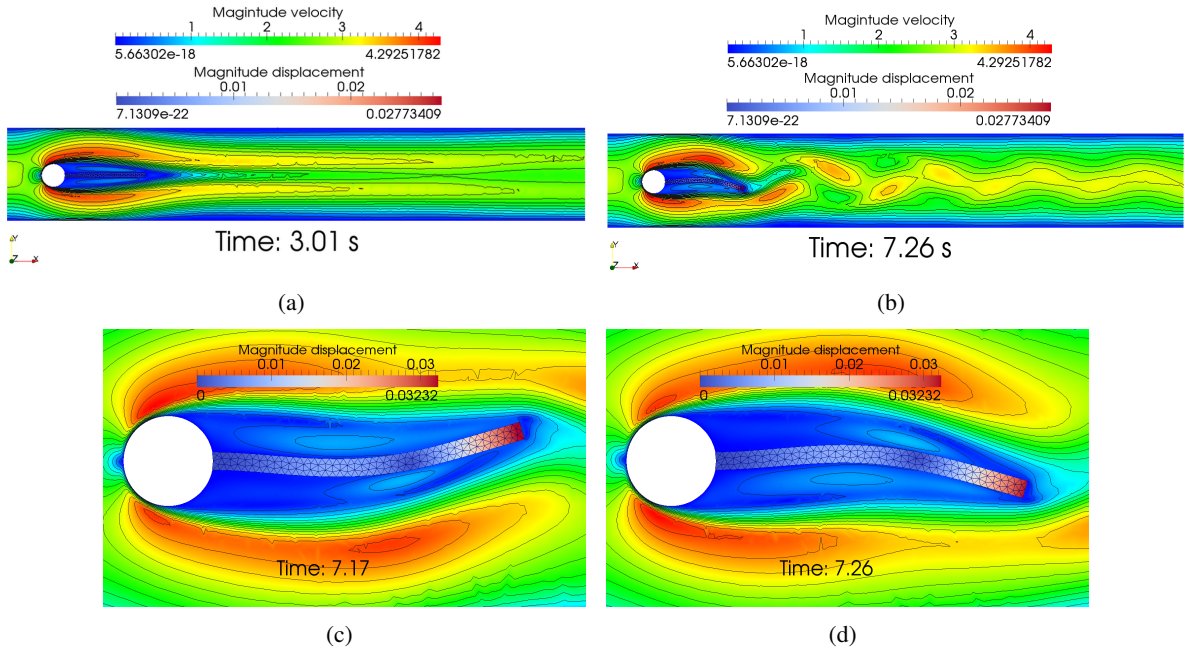


Figure 7: Results for **FSI3** with the configuration (3)

6. Blood flow applications

We describe now a 2D and 3D benchmark in the blood flow context which are simulating the propagation of a pressure pulse through a pipe. In both cases the minimal CIP stabilization strategy is used to control the velocity at the inlet. For the 2D case, we have chosen $\mathcal{F} = \mathcal{F}_h^i \cap \{\mathbf{x} \in \mathbb{R}^2 : (\mathbf{x}_{in} - \mathbf{x}, \mathbf{n}_{in}) \leq 0\}$, with $\mathbf{x}_{in} = (0.3, 0)$. For the 3D case, we stabilize only on the faces of the inlet, i.e. $\mathcal{F} = \Gamma_{in} \cap \mathcal{F}_h^b$.

6.1. 2D Benchmark

The geometry is a rectangle of 6 cm long by 1cm. In this particular case, we use a 1D reduced model for the structure, the *generalized string model*, using the discretization as in [5]. The purpose of this simulation is to show that under realistic parameters, the minimal CIP stabilization, as well as the high order approximation for both fluid and structure provide satisfactory results.

We plot the flow rate and average pressure at various cross sections of the flow for several timesteps in Figure 9. The results are in good agreement with [15].

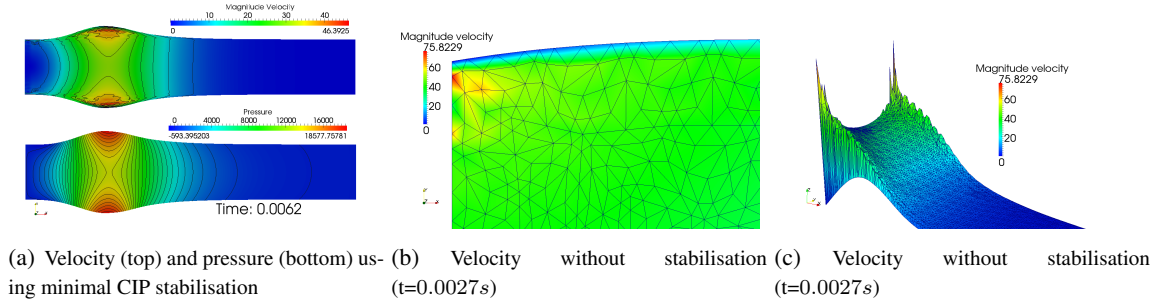


Figure 8: Simulation using a $P_c^4(\Omega_{f,(h,3)}) \times P_c^3(\Omega_{f,(h,3)})$ fluid discretisation, $V_{s,(h,1)}^3$ for the structure and timestep $\Delta t = 10^{-4}$. All other parameters are taken from [15].

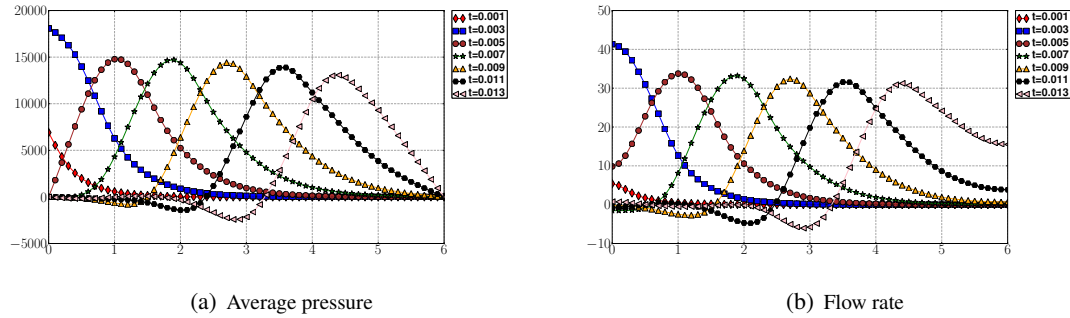


Figure 9: Average pressure and flow rate at various cross-sections of the flow and various time steps.

6.2. 3D Benchmark

Finally we present a blood flow application in large arteries, as presented in [16]. The geometry is a straight pipe of size $Lg = 6$ with an axis $(1, 0, 0)$ and a radius 0.5 . A pressure pulse $1.3332 \times 10^4 g / (cm s^2)$ has been imposed at the inlet boundary during $0.003s$. The thin elastic vessel ($0.1cm$) is clamped at the inlet and outlet. Figure 10 displays the radial displacement at various points of the FSI interface while figure 11 shows the pressure wave propagation for different time steps. We have used a $P_c^3(\Omega_{f,(h,2)}) \times P_c^2(\Omega_{f,(h,2)})$ space for the fluid and $V_{2,(h,2)}$ for the structure. The time scheme for the fluid is a BDF scheme of second order.

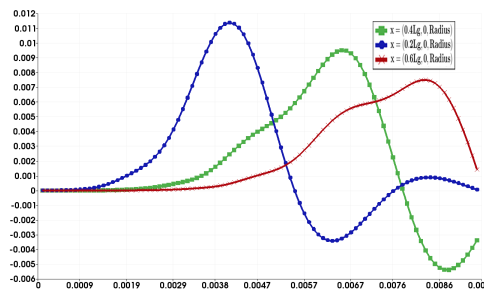


Figure 10: Radial displacement for several points on the fsi interface

Again the results are in agreement with [16] however a more thorough benchmarking is needed.

7. Conclusion

We have now a complete high order fluid-structure interaction framework in 2D and 3D. However much remains to be done in various areas. Indeed we need to make a thorough study of our Navier-Stokes in moving domains framework in terms of approximations — the Arbitrary Lagrangian Eulerian framework in particular — as well the underlying linear algebra solvers updating the results of our previous paper [2]. The FSI framework needs also to be more thoroughly benchmarked specially in 3D however there are no available benchmarks to our knowledge. Also, in the three dimensional case, a

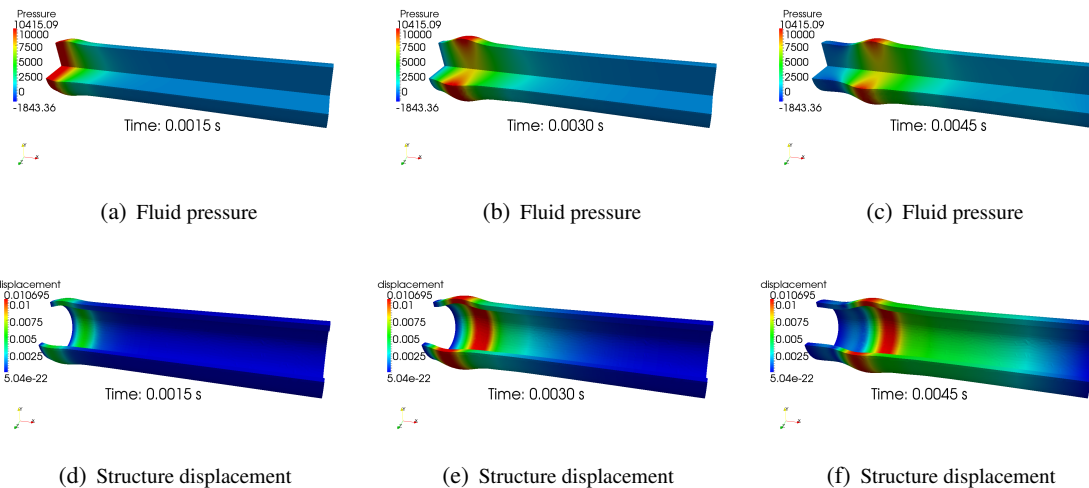


Figure 11: Pressure wave in a straight pipe. We show the fluid pressure and the fluid displacement of the pipe is magnified 10 times.

more robust strategy for the first step of the ALE map is under investigation. Finally the conjecture on the properties of our ALE discrete map should not be very difficult to actually prove.

Acknowledgments. The authors would like to thank the Région Rhône-Alpes (ISLE/CHPID project) as well as the french National Research Agency (MOSICOB and Cosinus-HAMM projects) and the Calouste Gulbenkian Foundation (*Estímulo à Investigação* project) for their financial support.

References

- [1] G. Pena, C. Prud'homme, Construction of a high order fluid-structure interaction solver, *J. Comput. Appl. Math.* 234 (7) (2010) 2358–2365.
- [2] G. Pena, C. Prudhomme, A. Quarteroni, High order methods for the approximation of the incompressible navierstokes equations in a moving domain, *Computer Methods in Applied Mechanics and Engineering* 209212 (0) (2012) 197 – 211. doi:10.1016/j.cma.2011.09.016.
URL <http://www.sciencedirect.com/science/article/pii/S0045782511003124>
- [3] C. Prud'homme, *Life: Overview of a unified C++ implementation of the finite and spectral element methods in 1d, 2d and 3d*, 2007.
- [4] C. Prud'homme, A domain specific embedded language in C++ for automatic differentiation, projection, integration and variational formulations.
- [5] G. Pena, Spectral element approximation of the incompressible Navier-Stokes equations evolving in a moving domain and applications, Ph.D. thesis, École Polytechnique Fédérale de Lausanne, n°4529 (November 2009).
URL <http://library.epfl.ch/theses/?nr=4529>
- [6] C. Prud'Homme, V. Chabannes, V. Doyeux, M. Ismail, A. Samake, G. Pena, *Feel++: A Computational Framework for Galerkin Methods and Advanced Numerical Methods*, submitted to ESAIM Proc. (Jan. 2012).
URL <http://hal.archives-ouvertes.fr/hal-00662868>
- [7] C. Prud'homme, V. Chabannes, G. Pena, *Feel++: Finite Element Embedded Language in C++*, Free Software available at <http://www.feelpp.org>, contributions from A. Samake, V. Doyeux, M. Ismail and S. Veys.
- [8] C. Geuzaine, J.-F. Remacle, Gmsh: a three-dimensional finite element mesh generator with built-in pre-and post-processing facilities, *International Journal for Numerical Methods in Engineering* 79 (11) (2009) 1309–1331.
- [9] W. J. Gordon, C. A. Hall, Construction of curvilinear coordinate systems and their applications, *Int. J. Numer. Meth. Eng.* 7 (1973) 461–477.
- [10] W. J. Gordon, C. A. Hall, Transfinite element methods: blending-function interpolation over arbitrary curved element domains, *Int. J. Numer. Meth. Eng.* 21 (1973) 109–129.
- [11] A. Winslow, Numerical solution of the quasilinear poisson equations in a nonuniform triangle mesh, *J. Comp. Phys.* 2 (1967) 149–172.
- [12] S. Turek, J. Hron, Proposal for numerical benchmarking of fluid-structure interaction between an elastic object and laminar incompressible flow, *Fluid-Structure Interaction* (2006) 371–385.
- [13] J. Hermansson, P. Hansbo, A variable diffusion method for mesh smoothing, *Communications in Numerical Methods in Engineering* 19 (2003) 897–908.
- [14] S. Balay, W. D. Gropp, L. C. McInnes, B. F. Smith, Efficient management of parallelism in object oriented numerical software libraries, in: E. Arge, A. M. Bruaset, H. P. Langtangen (Eds.), *Modern Software Tools in Scientific Computing*, Birkhäuser Press, 1997, pp. 163–202.

- [15] F. Nobile, Numerical approximation of fluid-structure interaction problems with application to haemodynamics, PhD, Ecole Polytechnique Fédérale de Lausanne, Switzerland.
- [16] L. Formaggia, A. Quarteroni, A. Veneziani, Cardiovascular Mathematics: Modeling and simulation of the circulatory system, Springer Verlag, 2009.